COMMUNICATION

Metal Driven Folding and Assembly of Minimal β-sheet into 3D-Porous Honeycomb Framework

Received 00th January 20xx,
Accepted 00th January 20xx

DOI: 10.1039/x0xx00000x

Nikhil Bajpayee,[a] Salil Pophali,[a] Thangavel Vijayakanth,[b] Shyamapada Nandi,[c] Aamod V. Desai,[d] Vinod Kumar,[e] Rahul Jain,[a] Santu Bera,[f] Linda J. W. Shimon,*[g] and Rajkumar Misra*[a]

In contrast to short helical peptides, constrained peptides, and foldamers, design and fabrication of crystalline 3D frameworks from the β-sheet peptides are rare because of their high self-aggregation propensity to form 1D architectures. Herein, we demonstrate the formation of 3D porous honeycomb framework through the silver coordination of minimal β-sheet forming peptide having terminal metal coordinated 4- and 3-pyridyl ligand.

Development of artificial, self-organized three-dimensional (3D) framework structures from biomolecular building blocks such as proteins/peptides have evolved for a broad range of applications in the fields of molecular recognition, separation, catalysis, materials and biomedical sciences. As metal ions are ubiquitous in nature, the concept of metal-coordinated self-assembly was introduced to simplify the design rule of 3D porous frameworks based on multiple hydrogen-bonds and hydrophobic interactions.[1] Initially, ultra-short peptides lacking defined secondary structures were employed for metal coordination and were shown to produce exciting adaptable, and tunable porous crystalline frameworks.[2] With the advent of chemical tools for sequence engineering of defined structure, there is rapid progress in the development of helical conformation based metal-coordinated framework using longer peptides such as collagen and coiled-coil peptides, short peptides (Pro-rich), and foldamers.[3]

On the other hand, β-sheets are a major structural motif observed in natural proteins and their interactions play crucial role in protein dimerization and oligomerization, protein-protein interaction, and peptide/protein aggregation.[4] Comprehending intermolecular interaction of β-sheets is not only important for protein folding, but also holds significant relevance in the realm of proteinopathies and therapeutics. For instance, amyloidosis, one of the greatest health threats of the 21st century, is characterized by the accumulation of amyloid fibrils caused by the uncontrolled aggregation of β-amyloid (Aβ) peptide through cross-β structure formation.[5] Moreover, β-sheets also serve as a valuable resource for the development of peptide based materials for bionanotechnological applications.[6] Concurrently, in living systems, 3D cylindrical self-assembly of β-sheets into β-barrels are one of the two pure protein tertiary structures that acts as binding proteins, pores, and enzymes in many variations.[7] While fabrication of 1D filamentous or fibrous stochastic assemblies from β-sheets is relatively common, generation of artificial crystalline 3D porous frameworks is highly challenging.

In this context, metal-coordinated self-assembly of β-sheets could reveal an important development in the goal to achieve 3D porous architecture. Suitable natural amino acids-based metal coordinating side chains or artificial metal binding ligands can be installed into the peptide strand to participate in the metal coordination and drive the polymerization process to form crystalline 3D supramolecular networks. Recently, Sawada et al. judicially utilized metal-coordinated self-assembly to artificially construct steric zipper arrangement of β-sheets which is a common hydrophobic packing in amyloid fibrils.[8] Nowick et al. strategically incorporated N-methylated amino acids in one of the β-strand of artificial macrocyclic β-sheet and demonstrated that 3D crystalline frameworks can be fabricated from the metal directed self-assembly of macrocyclic β-sheets.[9] Furthermore, Fujita et al. have presented the construction of artificial β-barrel structures having large cylindrical pores through metal driven assembly of octapeptides comprising of β-strand and loop-forming sequences.[10] However, the existing literature offers only limited evidence and understanding on the metal-directed self-assembly of minimal β-sheet forming peptides into diverse complex structures, such as 3D crystalline porous honeycomb frameworks.

Herein, we report the design, synthesis and metal-directed

[a] Department of Medicinal Chemistry, National Institute of Pharmaceutical Education and Research (NIPER), Mohali, S.A.S. Nagar (Mohali) 160062, India. E-mail: rkmisra@niper.ac.in
[b] The Shmunis School of Biomedicine and Cancer Research, George S. Wise Faculty of Life Sciences, Tel Aviv University, 6997801 Tel Aviv, Israel
[c] Chemistry Division, School of Advanced Sciences, Vellore Institute of Technology, 600127, Chennai, India
[d] School of Chemistry, University of St Andrews, North Haugh, St Andrews KY16 9ST, United Kingdom
[e] Department of Pharmacology and Toxicology, National Institute of Pharmaceutical Education and Research, Sector 67, S. A. S. Nagar, Punjab 160 062, India
[f] Department of Chemistry, Ashoka University, Sonipat, Haryana 131029, India
[g] Department of Chemical Research Support, The Weizmann Institute of Science, 7610001, Rehovot, Israel. E-mail: Linda.Shimon@weizmann.ac.il
† Electronic Supplementary Information (ESI) available. See DOI: 10.1039/x0xx00000x

higher order self-assembly of two minimal tripeptides having different coordinating sites into 3D crystalline porous honeycomb frameworks with well-defined porous channels and supramolecular metallogel with impressive mechanical properties.

In order to understand the metal-driven construction of complex 3D architecture, two short peptides **P1** and **P2** as depicted in Scheme 1 were designed and synthesized. Both 3- and 4-pyridyl metal binding ligands were used to examine the influence of coordinating sites on the metal driven folding and assemblies of these short peptides. All the peptides were synthesized in solution phase fragment condensation strategy, purified through reverse phase HPLC, and characterized by mass spectrometry and nuclear magnetic resonance (NMR).

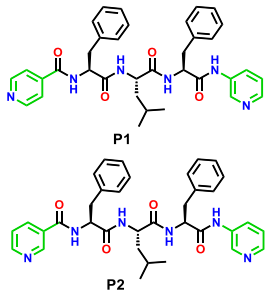

Scheme 1 Sequence and chemical structure of short β-sheet forming tripeptides.

To understand the unambiguous conformations of peptide ligand **P1**, we subjected crystallization in different conditions. Unfortunately, we were unsuccessful in obtaining single crystals of peptide **P1**, and thus 2D NMR spectroscopy were employed to comprehend the conformational preferences. The analysis of the ROESY spectrum (DMSO-d_6 at 298 K) of **P1** showed very weak NH↔NH ROEs, however, existence of strong CαH ↔ NH ROEs between *i* and *i+1* residues, supported the extended conformation (Fig. S1-S3).[11] Folding and assembly of **P1** upon coordination to Ag^{I} was investigated after growing the single crystals of **P1**-$AgBF_4$ complex. Fourier-transform infrared (FTIR) analysis was performed of the isolate metal-peptide crystals to understand the secondary structure of ligand in a metal complex which showed sharp amide I band at 1638 cm^{-1} demonstrating the presence of predominate β-sheet conformation (Fig. S4).[12] Further, a single crystal of **P1**-$AgBF_4$ complex suitable for diffraction was subjected to an X-ray diffraction study. Diffraction data was collected to 0.90 Å resolution and refined in the R32 space group. Atomic level structural analysis revealed that in the asymmetric unit, two nearly-identical **P1** monomer subunits (P1A and P1B) are connected in a head-to-head fashion through linear 4py–Ag–4py coordination and crystallized with one BF_4^- counterion (Fig. 1a). In the individual **P1** unit, the two aromatic side chains of Phe residues are arranged in the same face relative to the peptide backbone, while the Leu side chain and pyridyl termini are displayed on the opposite side of the peptide backbone (Fig. 1a). The torsion angles around the Leu2 residue appeared to play a pivotal role in dictating the overall structural feature of the peptide backbone. The allowed torsion angles of the Leu2 residue were found to be localized within the extended β-sheet region of the Ramachandran plot, with ϕ2 and ψ2 values of -152° and 158° for P1A and -129° and 149° for P1B, respectively (Supplementary Table S1). Individual β strands are further interacted with the adjacent strands that are oriented in an antiparallel fashion thereby forming a supramolecular antiparallel β-sheet structure.[6] Figure 1b displays the consensus pattern of hydrogen bonding (average N···O distance of 2.85 Å in strand P1A and 2.83 Å in strand P1B) between strands in each of the antiparallel sheets illustrating that their organization allows for pairing of nearly all intermolecular backbone hydrogen-bonds. Further stabilization of the β-sheet conformation is achieved through aromatic-aromatic interactions between the phenyl ring of Phe3 residue of one strand with the 4Py motif of next strand (center-center distance= 4.56 and 5.73 Å for P1A and P1B, respectively). This in turn forces the 3Py motif adjacent to Phe3 to reside in a bending position as compared to the remaining backbone of the strand. In this arrangement of strands, aromatic residues (Phe1, Phe3) appear on one face of the dimeric β-sheet while Leu2 side chain acquires the other face. Further assembly of these sheets along both faces can form a dry interface and stabilize through tight interactions in the self-complementary association of the hydrophobic side chains like that of steric zippers.[8]

More intriguingly, the NH and CO groups of the Phe1 residue of each β-strand form intermolecular hydrogen bonds with the NH and CO groups of the Phe1 residue in the adjacent strand (N5…O7=2.91 Å and N11…O3=2.88 Å (Fig. 1c). This, coupled with the strong π-π stacking interaction between the 4-pyridyl group (centroid-centroid distance 3.842 Å) and metal coordination (4Py-Ag-4Py), results in the formation of a triangular structure with a central channel (Fig. 1c). Moreover, within the triangular structure, each silver ion is further coordinated with C-terminal pyridine of another two β-strands to form a tetrahedral complex (Fig. 1d).

Each strand of the tetrahedral complex forms intermolecular H-bonds with adjacent β-strands to produce the dimeric β-sheet structures. The overall packing results in a hexameric assembly of β-sheets and produce a channel like structure (internal diameter of 6.32 Å) along c axis (Fig. 1e). In converse to the general affinity of β-sheets to form 1D supramolecular polymers, the current 3D assembly of artificial β-sheets into well-defined supramolecular oligomers is rare and comparable to the formation of artificial β-barrel structure (Fig. 1e and 1f).[10] In the organization of barrel-like hexamer, aromatic residues (Phe2 and 4-Py) are extended towards the cavity and creating a hydrophobic core inside the hexamer. Both metal coordination and aromatic-aromatic interactions play a significant role in stabilizing the overall structure of the framework. Due to suitable volume and perfectly fitting into the void space, the counter anions of the Ag salt, BF_4^- are encapsulated inside the pore and thereby blocking the channels. In the higher order packing, utilizing metal coordination and hydrophobic stacking each dimeric β-sheet participates in two another kind of pore formation along with one discussed above. The opposite end of the β-sheet that did not participate in the hexameric pore formation, coordinates in two different ways. The 3Py motif

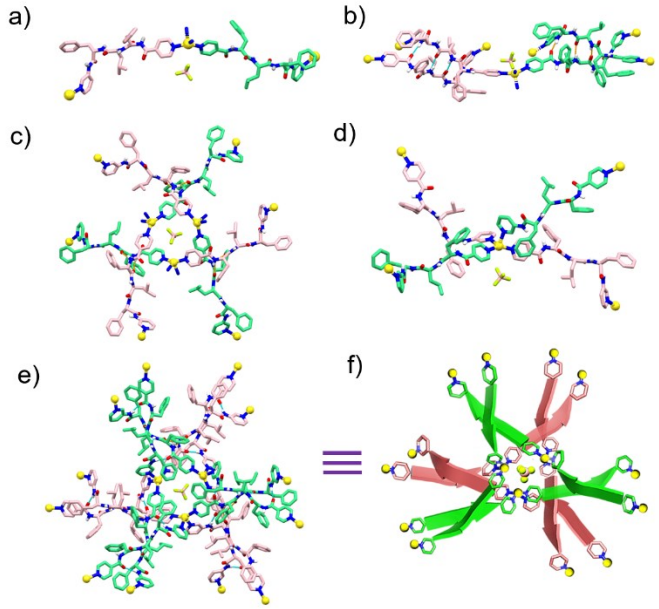

Fig. 1 a) Atomic structure of silver coordinated **P1**. b) Observed inter-strand backbone hydrogen bonds. c) Formation of triangular structure through H-bonds and metal coordination between the β-strands. d) Tetrahedral silver complex formation via coordination of four β-strands. e) β-barrel like assembly of six β-sheet through silver coordination (top view) and its carton representation.

interacts in head-to-tail fashion with adjacent β-sheet through 3Py-Ag-3Py coordination and organizes in helical structural arrangement (Fig. S6).

Three β-sheet units complete a helical turn and five such units fabricate the internal cavity of helical structure. The overall packing extends six Leu2 residues towards the cavity and thus produces a hydrophobic core of diameter 8.49 Å (Fig. S6). This end of the β-sheet further interacts with another adjacent β-sheet through both pyridyl motifs in 3Py-Ag-4Py and 4Py-Ag-3Py fashion and fabricates another helical structural arrangement (Fig. S7). Top view of the helical structure displays the formation of nearly circular cavity with an average diameter of 3.99 Å (Fig. S7). The supramolecular arrangement situates amide groups at the inner edge of the pore, enhancing accessibility for hydrophilic guests. Excitingly, the higher order packing of the **P1**-$AgBF_4$ complex along the c-axis has resulted in a 3D porous honeycomb-like framework comprising of three distinct pores, each distinguish by its unique size and nature (Fig. 2). The voids for the structure as mapped by contact surface (probe radius 1.2 Å) indicate a void volume of 19984 $Å^3$, which is ~42% of the unit cell volume (calculated by Mercury).[13] Attempt to study gas adsorption capability of the framework under vacuum showed insignificant amount of N_2 or CO_2 uptake (Fig. S8). However, peptide-based frameworks comprising flexible ligands could exhibit different classes of porosity like static porosity, dynamic porosity, and cooperative porosity with diverse nature of stability suitable for biotechnological applications such as catalysis, selective encapsulation, and tissue engineering.[14] The thermal stability of the **P1**-$AgBF_4$ porous framework was evaluated using thermogravimetric analysis (TGA), revealing no significant mass change up to 300 °C, indicative of its good thermal stability (Fig. S9).

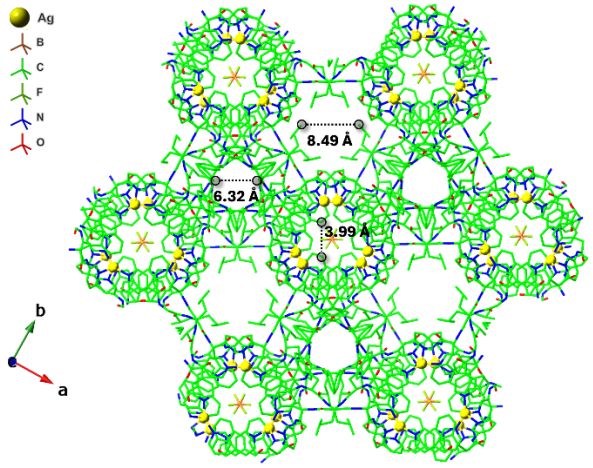

Fig. 2 3D porous honeycomb like structure from the higher order assembly of [($AgBF_4$)·**P1**] n complex.

From the above observation it is clear that the coordination mode of 4-pyridyl nitrogen plays a significant role in the higher-order structure formation of [($AgBF_4$)·**P1**]n complex. Further, to understand this phenomenon in more detail, we have synthesized the same sequence only replacing N-terminal 4-pyridine by 3-py (**P2**). Like **P1**, **P2** has a latent property to form extended structure which was further supported by 2D-NMR spectroscopy. The absence of NH ↔NH ROEs and presence of strong CαH ↔ NH ROEs in ROESY spectrum, providing evidence for the extended type of conformation (Fig. S10).[11] Interestingly, when ethanolic solution of **P2** (250 µL of 30mM of **P2** in EtOH) was added to 250 µL of 30 mM of aqueous solution of $AgBF_4$ in a glass vial and kept for few minutes after sonication, formation of a stable gel was observed.[15] This was confirmed by the vial inversion method (Fig. 3a). The mechanical properties of metallogel were evaluated by rheological measurements.[16] Dynamic frequency sweep (at 0.1% strain over 0.1–100 Hz) revealed the linear viscoelastic region. The greater storage modules (G′) compared to the loss modulus (G′′) across a wide range frequency confirming its viscoelastic nature (Fig. 3b). In addition, a strain sweep experiment at a constant frequency of 1Hz demonstrated that as the strain increased, gel ruptured, and at 17% strain, complete gel rupture occurred (Fig. 3c). To comprehend the morphological features of the metallogel, transmission electron microscopy (TEM) was employed (Fig. 3d). The result revealed that the metallogel is comprised of entanglements of fibrillar networks. FTIR analysis of the dried metallogel exhibited amide I band at 1637 cm^{-1} indicating β-sheet mediated aggregation in the gel state (Fig. S11).[12] Moreover, we performed X-ray powder diffraction of lyophilized gel samples which showed broad diffraction peaks at 4.2 and ~10.5 ° that are consistent with cross-β structure pattern of amyloid fibril (Fig. S12).[17] Intriguingly, upon exposure to ambient light, the transparent metallogel changed to a light brown color indicating the formation of silver nanoparticles (Fig 3e inset), which was further supported by TEM micrographs (Fig. 3e, S13).[18] It is noteworthy to mention that our different extensive attempts to crystalize the [($AgBF_4$)·**P2**]n complex were not successful. This could be due to the natural tendency of the

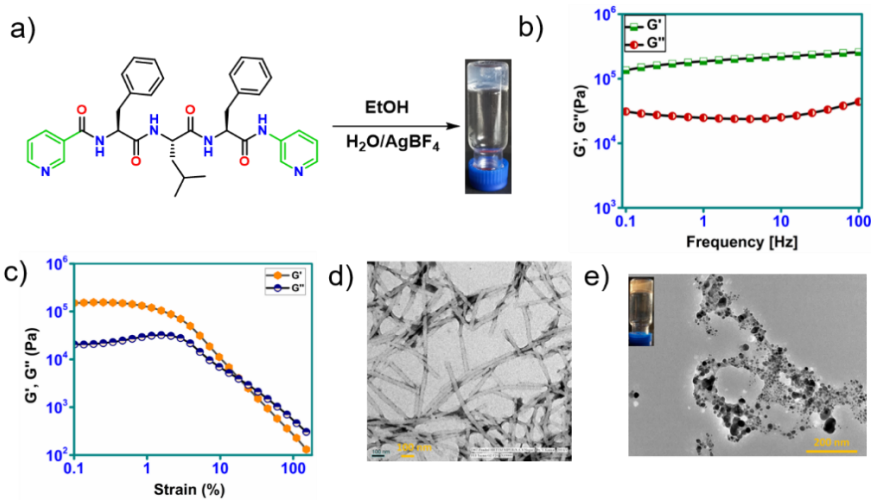

Fig 3. a) Formation of silver metallogel. b) Frequency-dependent oscillatory rheology of metallogel at 0.1% strain. c) Step-strain time-dependent rheological analysis of metallogel at constant frequency 1Hz. d) TEM image of the metallogel. e) TEM images of metallogel after exposure of day light revealing silver nanoparticle formation, digital image (inset).

P2 to form a linear complex with di-coordinated Ag instead of forming the tetra-coordinated Ag in the $[(AgBF_4)\cdot\mathbf{P1}]_n$ complex. This clearly indicating the fact that the presence of the 3- and 4-pyridyl binding site in the C and N terminal of the peptide sequence is crucial to isolate the crystalline 3D framework materials.

In summary, we have showcased the successful development of crystalline 3D-porous honeycomb framework from the metal driven folding and higher order assembly of a minimal β-sheet forming peptide. Using two different metal binding sites at the two termini, it was possible to direct the metal coordinated self-assembly process of β-sheets into β-barrel like architecture. Furthermore, we have also demonstrated how slight alteration of the ligand induces a shift in the metal-driven self-assembly process, transitioning it from a 3D crystalline framework to supramolecular fibrillar networks. This observation holds significant importance in unravelling the design principles of this new class of systems and providing guidance for the metal driven self-assembly of β-sheets into 3D frameworks.

This research was supported by the DST Inspire Faculty Fellowship (No. DST/INSPIRE/04/2020/002499) from the Department of Science and Technology, New Delhi and National Institute of Pharmaceutical Education and Research, S. A. S. Nagar. S.B. thanks SERB, Govt. of India for the Ramanujan Fellowship (Ref. no. RJF/2022/000042) and Ashoka University, Sonipat, Haryana for the infrastructure. Authors are thankful to Dr. Sangita Roy and Sourav Sen (INST Mohali) for their help in the Rheological measurement.

Conflicts of interest

There are no conflicts to declare.

Notes and references

1 (a) D. Huard, K. Kane, F. Tezcan, *Nat Chem Biol*. 2013, **9**, 169–176; (b) J. Aupič, F. Lapenta, Z. Strmsek, E. Merljak, T. Plaper, R. Jerala *Sci. Adv*. 2022, **8**, eabm8243; (c) J. Dong, Y. Liu, Y. Cui, *J. Am. Chem. Soc.* 2021, **143**, 17316 17336. (d) N. Bajpayee, T. Vijayakanth, S. R-Lazar, S. Dasgupta, A. V. Desai, R. Jain, E. Gazit, R. Misra, *Angew. Chem. Int. Ed*. 2023, e202214583.

2 J. Rabone, Y.-F. Yue, S. Y. Chong, K. C. Stylianou, J. Bacsa, D. Bradshaw, G. R. Darling, N. G. Berry, Y. Z. Khimyak, A. Y. Ganin, P. Wiper, J. B. Claridge, M. J. Rosseinsky, *Science* 2010, **329**, 1053–1057.

3 (a) M. M. Pires, J. Chmielewski, *J. Am. Chem. Soc*. 2009, **131**, 2706 2712; (b) T. Schnitzer, E. Paenurk, N. Trapp, R. Gershoni-Poranne, H. Wennemers, *J. Am. Chem. Soc*. 2021, **143**, 644–648; (c) T. Sawada, M. Fujita, *Chem.* 2020, **6**, 1861–1876; (d) R. Misra, A. Saseendran, S. Dey, H. N. Gopi, *Angew. Chem. Int. Ed*. 2019, **58**, 2251– 2255; (e) S. Jeong, L. Zhang, J. Kim, J. Gong, J. Choi, K. M, Ok, Y. Lee, S. Kwon, H.-S. Lee, *Angew. Chem., Int. Ed*. 2022, **61**, e202108364.

4 P.-N. Cheng, J. D.Pham, J. S. Nowick, *J. Am. Chem. Soc*. 2013, **135**, 15, 5477–5492

5 T. P. J. Knowles, M. Vendruscolo, C. M. Dobson, *Nat. Rev. Mol. Cell. Biol*. 2014, **15**, 384-396.

6 (a) A. Levin, T.A. Hakala, L. Schnaider, G. J. L. Bernardes, E. Gazit, T. P. J. Knowles, *Nature Reviews Chemistry* 2020, **4**, 615–634; (b) S. Kim, J. H. Kim, J. S. Lee, C. B. Park, *Small* 2015, **11**, 3623-3640.

7 S. W. Cowan, T. Schirmer, G. Rummel, M. Steiert, R. Ghosh, R.A. Pauptit, J. N. Jansonius, J. P. Rosenbusch, *Nature* 1992, **358**, 727.

8 E. Tsunekawa, Y. Otsubo, Y. Yamada, A. Ikeda, N. Adachi, M. Kawasaki, A. Takasu, S. Aramaki, T. Senda, S. Sato, S. Yoshida, M. Fujita, T. Sawada, *J. Am. Chem. Soc*. 2023, **145**, 16160–16165.

9 W. J. Howitz, M. Wierzbicki, R.W. Cabanela, C. Saliba, A. Motavalli, N. Tran, J. S. Nowick, *J. Am. Chem. Soc*. 2020, **142**, 15870– 15875

10 M. Yamagami, T. Sawada, M. Fujita, *J. Am. Chem. Soc.* 2018, **140**, 8644–8647.

11 R. Misra, R. M. Reja, L. V. Narendra, G. George, S. Raghothama, and H. N. Gopi, Chem. Commun., 2016, **52**, 9597-9600

12 J. Kong, S. Yu. *Biochim. Biophys. Sin*. 2007, **39**, 549–559.

13 L. J. Barbour, *Chem. Commun*., 2006, 1163–1168

14 J. R. Holst, A. Trewin and A. I. Cooper. *Nat. Chem*. 2010, **2**, 915-920

15 J. A. Foster, M.-O. M. Piepenbrock, G. O. Lloyd, N. Clarke, J. A. K. Howard, J. W. Steed, *Nat. chem*. 2010, **2**, 1037-1043.

16 C. Yan and D. J. Pochan, *Chem. Soc. Rev*., 2010, **39**, 3528– 3540

17 D. A Kirschner, C. Abraham, and D. J Selkoe Proc. *Natl. Acad. Sci. USA,* 1986, **83**, 503-507

18 K. Nath, A. Husain and P. Dastidar, *Cryst. Growth Des*., 2015, **15**, 4635